Chapter 2

Experiments

One of the first experiments involving a particle colliding with a stationary wall in a viscous liquid environment was performed by McLaughlin (1968) who found that the rebound trajectory was shown to depend on the particle impact Reynolds number. His experiments, however, were performed over a small range of Reynolds numbers. Barnocky & Davis (1988) dropped solid particles of a few millimeters in air onto a solid plate that was covered by a thin liquid layer (about $0.1 \sim 0.5$ mm thick) and observed if the particles rebounded or not. To ensure a rebound, the sphere needs to possess sufficient inertia to overcome the hindering fluid effect for a non-zero velocity upon contact. As the viscosity and the thickness of the liquid layer was increased, a greater critical drop height was need for the occurrence of a particle rebound. They did not measure the coefficient of restitution above the transition but obtained a critical Stokes number for rebound, St_c, from approximately 0.25 to 4 for smooth surfaces. Lundberg & Shen (1992) studied the dependence of the coefficient of restitution upon the fluid viscosity for the collision of a roller attached to a pendulum with a fixed ball covered by a thin layer of viscous oil. They found that for oil with moderate values of viscosity to 0.01 Pa·s, the restitution coefficient is similar to that in a dry collision. However, at higher values of viscosity, the restitution coefficient can become much less. This dependence on viscosity is stronger for softer material where the surface deformation is larger, resulting in an increased contact surface area and thus higher effect of the viscous dissipation. Zenit & Hunt (1999) and Joseph *et al.* (2001) investigated the collisions totally immersed in a viscous fluid with a pendulum-like apparatus that permits a horizontal impact motion towards a vertical wall. A critical Stokes number, $St_c = 10$, for

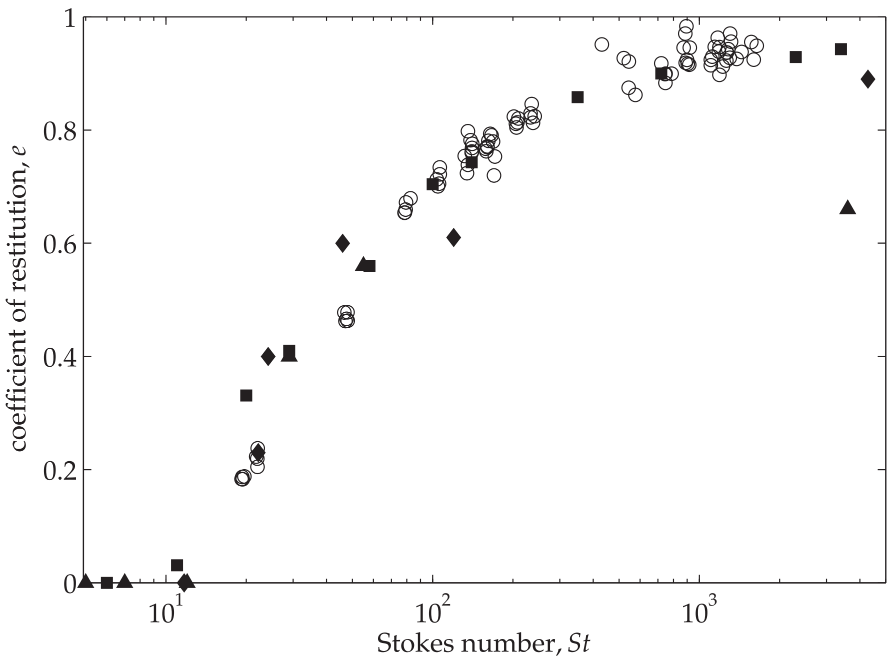

Figure 2.1: Coefficient of restitution, e, as a function of Stokes number. 'o' for steel particles impacting a Zerodur wall in Joseph *et al.* (2001); '♦' for steel ball bearings impacting an anvil in McLaughlin (1968); '▲' and '■' for steel spheres impacting a glass wall in Gondret *et al.* (1999) and Gondret *et al.* (2002).

the bounce transition was observed. The surface roughness of the materials was found to impact the value of coefficient of restitution for $St < 80$. Gondret *et al.* (2002) performed similar experiments to McLaughlin's using a solid sphere falling under gravity in a fluid onto a solid wall. The dependence of the coefficient of restitution upon the particle Stokes number showed similar trend with McLaughlin (1968) and Joseph *et al.* (2001)'s results, as shown in figure (2.1) which is taken from figure (3.7) of Joseph (2003).

For collisions with high Stokes number, the viscous force is small compared with the particle inertia, resulting in a near unity coefficient of restitution. The small value (around 0.7), as shown by the filled triangle at Stokes around 4000, is a result from Gondret *et al.* (1999) who claimed 3 years later that 'the point appears to be underestimated due to the previous data analysis which has been proved to be too crude for high St' (see Gondret *et al.*, 2002) With decreasing Stokes number, the coefficient of restitution drops from unity. When the Stokes number is smaller than a critical value, a restitution coefficient is zero, indicating no rebound happens, at least within the experimental resolution of the image acquisition system.

The aforementioned experiments mainly focused on coefficient of restitution based on the behavior of a particle right before and after it collides with a wall. In Joseph *et al.* (2001) pendulum experiments, the trajectory and velocity profile were obtained. However, the surrounding flow field coupled with the pendulum motion of the sphere was three dimensional and computationally expensive to be simulated. Gondret *et al.* (2002) presented the rebound trajectory and velocity of a particle falling under gravity and colliding with a wall, which resulted in axisymmetric surrounding flow field; however, the initial trajectory of the particle after it is released was not included. In the experiments performed by TenCate *et al.* (2002), the whole process of a sphere settling toward a wall was recorded. The sphere was released from zero velocity while simultaneously triggering the camera to start filming until the sphere rested on the wall. The experimental results allowed the validation of a solution for the surrounding flow field which is directly coupled with the motion of the sphere during a settling process as described in Chapter 3. However, TenCate *et al.* (2002) did not include results for Stokes numbers greater than the critical value.

Thus, new experiments were performed to record a complete collision process in a viscous liquid including the trajectory of a particle as it accelerates from zero velocity after release, collides with a wall, rebounds and falls again until it comes to rest. The new experimental results provide a calibration for a proposed contact model described in Chapter 4 which captures the collision and rebound processes. Moreover, the experimental trajectories of the collisions with different Stokes numbers are compared with the simulated results. A detailed description of the motion of a particle especially when it is about to collide with a wall is obtained by using a CCD camera with a higher frame rate.

2.1 Experiment setup

2.1.1 Experiment apparatus

The experiment setup is shown schematically in figure (2.2). The experiments are performed in a glass rectangular tank with length×width×height as $600 \times 350 \times 450$ mm that contains a mixture of glycerol and water. A steel sphere with diameter $D = 9.5$ mm is dropped from an electromagnetic release mechanism that is fixed on the top of the tank. A trigger pad is used to cut off the current in the electromagnetic mechanism releasing the steel sphere from zero velocity under quiescent ambient fluid condition. The circular release surface with diameter 52 mm is immersed in the liquid a certain depth ($>$ 50 mm) under the free surface of the liquid, and the effect of the liquid free surface on the experiment is ignored. A cylinder-shaped Zerodur block with diameter 150 mm and height 100 mm is placed coaxially below the release mechanism from a certain distance as a target wall. Zerodur is a hard glass-like material and it can be polished to a high accuracy to minimize the effect of wall roughness on the experiments. A level is used to make sure the top surface of the Zerodur is horizontal. The release surface is kept parallel to the top surface of the Zerodur block. The sphere is dropped from the center of the release surface and falls along the axis of the Zerodur block. The dimension of the glass tank is large compared with the sphere diameter so that the flow field around the moving sphere can be considered as axisymmetric as long as the particle Reynolds number $Re = \frac{DV}{\nu}$ is less than 250. Moreover, the large dimensions of the tank allow the use of the far field boundary condition in the following simulation.

A high speed videography system (a high speed camera, a control/display monitor and a record trigger) is used to capture the particle dynamic behavior. Figure (2.3) shows an example image on the monitor with a control menu on the right. The camera frame rate is set to be 4000 frames per second so that the time interval between two successive frames is 0.25 ms. Under this frame rate, the resolution is 160 pixels wide by 140 pixels high. More details of the motion of a particle, especially when it is about to collide with the wall, can be obtained by using this higher frame rate. The shutter speed is 1× which allows the camera to capture as much light as possible. The filming

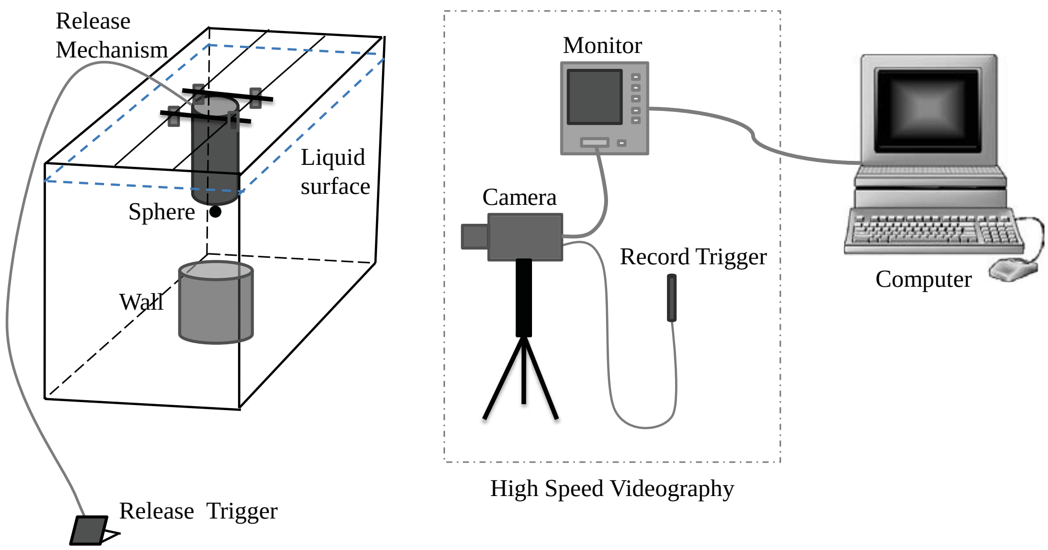

Figure 2.2: Schematic experiment setup

starts prior to the release of the sphere to avoid missing the initial part of the collision process since the release pad and the record trigger are controlled manually and separately. During playback, the frame rate is set at 30 frames per second because this is the rate at which MATLAB can digitize a video. The video recorded by the videography system is transferred into a computer as an output '.avi' file by using software 'VirtualDub' which captures the video playing on the control/display monitor.

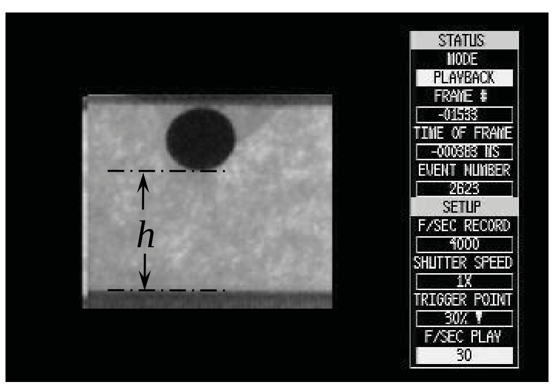

Figure 2.3: The image shown on the control/display monitor. h is the gap between the sphere and the wall.

2.1.2 Material properties

Steel spheres with diameter 9.5 mm are used in the experiments. The target wall is made of Zerodur. The properties of the solid material are listed in Table (2.1) including solid density, ρ_p, Young's modulus, E, Poisson's ratio, ν.

Material	ρ_p(kg/m^3)	E(GPa)	ν
steel	7780	200	0.33
Zerodur	2530	91	0.24

Table 2.1: Properties of the sphere and the wall used in the collision experiments

Aqueous glycerol solutions were used as the surrounding fluid for the experiments. Glycerol is completely miscible with water, which allows for a large range of viscosities to be explored by changing the mixture proportions. Also, the viscosity of the mixture varies significantly with temperature. Therefore, the liquid temperature is measured before each collision by a digital thermocouple thermometer. The apparent specific gravity of the liquid is measured by a hydrometer. Based on the measured temperature and apparent specific gravity, the concentration of the mixture can be found from the datasheets presented in Joseph (2003) that are readily available at Dow Chemical Synthetic Glycerin Products. Finally, the density and the viscosity of the liquid can be found from the datasheets based on the temperature and the concentration.

2.2 Experimental data process

The output video '.avi' file is first converted into DivX format by using software 'YasaVideoConverter'. The size of the video after conversion is much smaller (about 40 times) than the original one, but the quality is good. Then this DivX video can be read by MATLAB at a frame rate 30 fps and converted into images in '.jpg' form. Figure (2.4) presents the images extracted from a recorded video for event 2623. The time interval between the successive images shown in the figure is 34.25 ms. In figure (2.4), (a) shows the initial state in which the velocity of the particle just starts to fall and the flow field is static; (b) shows the particle moving under gravity towards the wall at a distance from the release surface; (c) is the moment when the particle collides with the wall and the distance

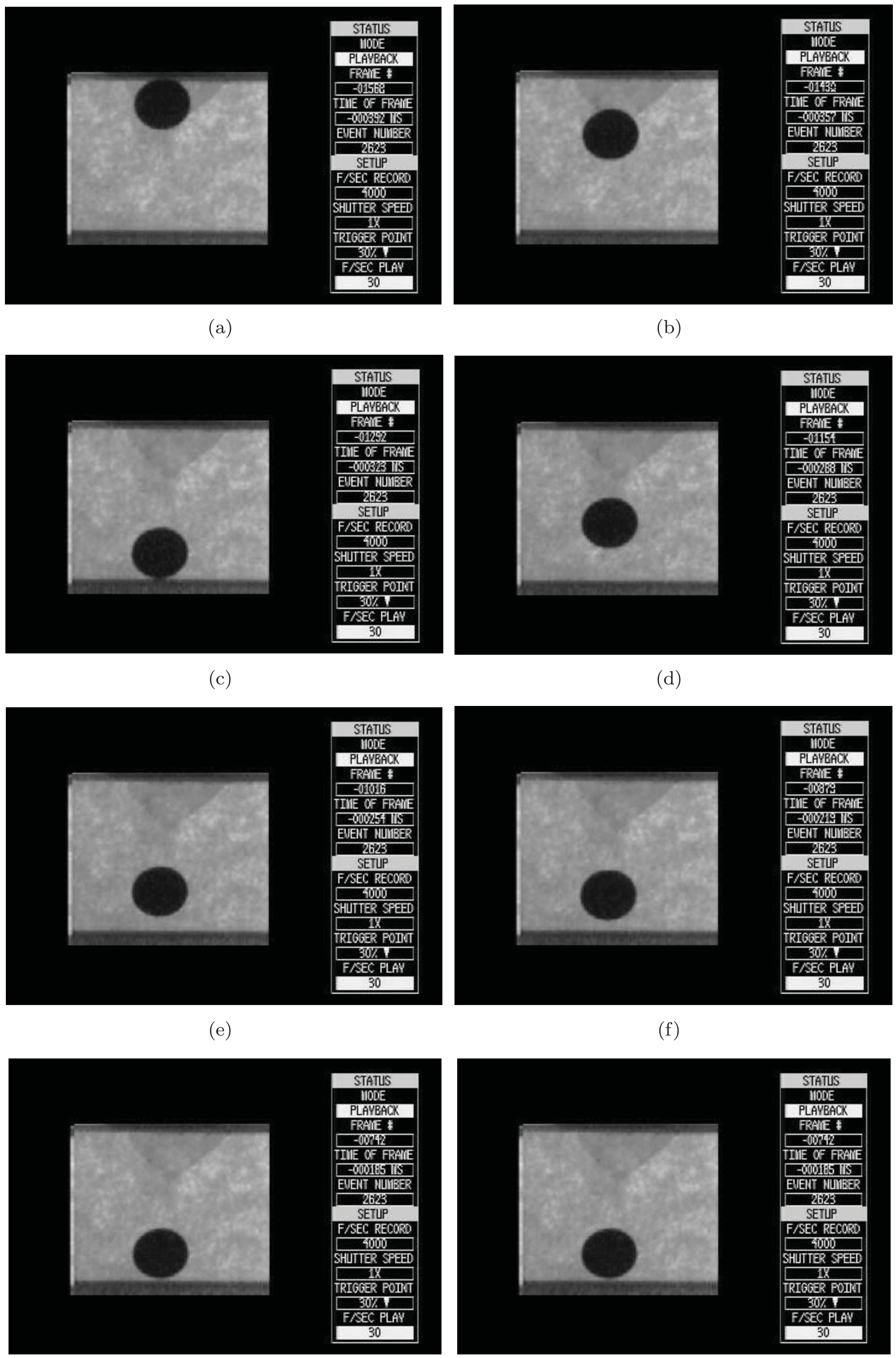

(a) (b)

(c) (d)

(e) (f)

(g) (h)

Figure 2.4: Images extracted from the recorded video

between the particle and the wall is zero; (d) shows the particle rebounding and approaching the maximum height; (e) shows the particle falling again toward the wall; (f) is the particle reaching the maximum height during the second rebound; (g) and (h) show the particle settling toward the wall and resting there.

To find the trajectory of a sphere, the images are analyzed with a template matching method that is widely used in digital image processing for finding incidence of a pattern or object within an image. For a single image, a region typically recognized as the sphere is manually cropped and saved as a template $T(x_t, y_t)$ where (x_t, y_t) represent the coordinates of each pixel in the template; then, the center of this template is moved over each point (x, y) in the image, and the normalized cross-correlation is calculated as

$$\frac{1}{n-1}\sum_{x,y}\frac{(F(x,y)-\bar{F})(T(x,y)-\bar{T})}{\sigma_T\sigma_T}$$

where n is the number of pixels in the template T and a subimage F. The position with the highest result is the best match and is considered as the position of the center of the sphere in the image. Applying this technique to a series of images (the same template can be used for images extracted from one video), the trajectory of the sphere can be found by relating the position of the sphere to the corresponding time for each image. For an example, the trajectory of the sphere in event 2623 is plotted in figure (2.5). The images shown in figure (2.4) are marked on the trajectory correspondingly. The position of the sphere plotted on the figure is the result of the position of the sphere center found from the above template matching technique minus the radius of the sphere. The unit is converted from ‘pixel’ to ‘mm’ by letting the template pixel correspond with the diameter of the sphere.

The velocity of the sphere calculated as the time derivative of the trajectory $\triangle h/\triangle t$ between the two successive images is plotted in figure (2.6). Large variations are obtained since the time interval 0.25 ms is small (compared with 2 ms in the experiments of Gondret *et al.* (2002) and 5∼10 ms in Joseph *et al.* (2001)), which amplifies the uncertainty of the experiment. Several steps have been

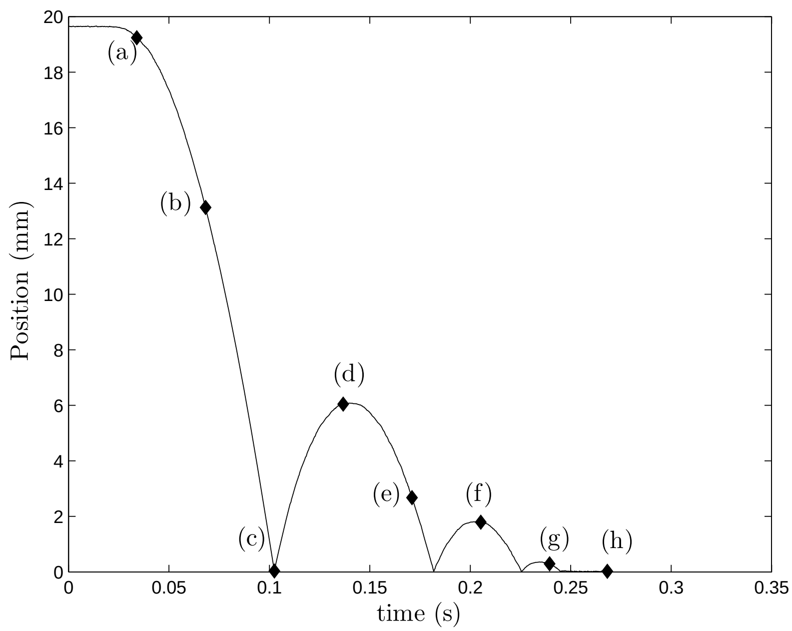

Figure 2.5: The trajectory of the sphere in event 2623. The diamond points show the corresponding position for the images in figure (2.4).

taken to diminish the vibration. First, for each collision process, the measurements were done three times which means that under the same condition, the sphere was dropped three times and three videos were recorded. The final trajectory is the average of the three trajectories obtained from the three videos. Then, for this averaged trajectory, when using the time derivative $\triangle h/\triangle t$ with $\triangle t = 2$ ms, the calculated velocity is much smoother, shown as the points in figure (2.7). An alternative is to fit the averaged trajectory with a high order (6th order) polynomial, $h = P(t)$, which keeps the characteristic shape of a trajectory but removes outlying points. Then, the velocity can be obtained by differentiating the polynomial and calculating the differential $V = \frac{dh}{dt}$ at different time step. The result of the alternative is shown by the lines in figure (2.7). Compared with the results given in Gondret *et al.* (2002)'s paper, the velocity profile in figure (2.7) shows not only the velocity of a sphere when it is about to collide with a wall and rebound, but also the acceleration process from zero initial velocity.

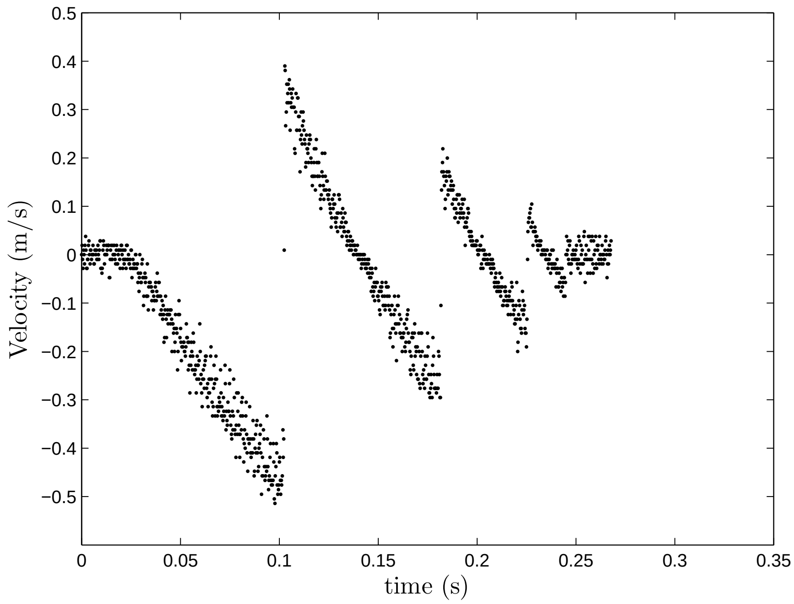

Figure 2.6: The velocity of the sphere in event 2623 calculated by using central difference of the trajectory with time interval 0.25 ms.

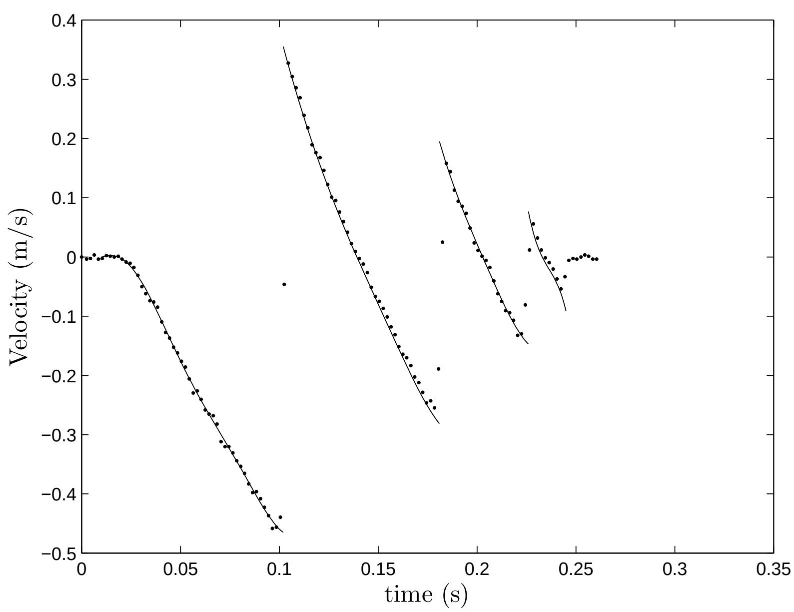

Figure 2.7: The velocity of the sphere in event 2623 calculated by using central difference of the trajectory with time interval 2 ms represented by points; the velocity profile calculated by fitting the experimental trajectory with polynomials represented by lines.

2.3 Experimental results

Collisions with different impact Stokes numbers were performed by placing the wall at different distances from the release surface. The apparent specific gravity of the liquid and the room temperature are measured for each experiment. A typical value of the apparent specific gravity is 1.205 when the room temperature is 20^oC. Thus, the concentration of the mixture is found to be 78% glycerol by weight, and the corresponding density and the viscosity of the liquid for that experiment are 1203 kg/m^3 and 50.2×10^3 Pa·s. After applying the above data process techniques, the trajectory and velocity of a sphere are obtained for each collision. The impact Reynolds number $Re = \frac{DV}{\nu}$ is calculated based on the impact velocity of the sphere which is the averaged value of the velocity obtained from the differential of the fitting polynomial over the 2 ms before collision. Because of the small values of $h(t = 0)/D$, where h is the gap between the particle and the wall as defined in figure (2.3), the particle does not achieve its terminal velocity before it contacts the wall. Thus, the particle Reynolds number is related to the fall distance. The Stokes number of each collision, $St = \frac{1}{9}\frac{\rho_p}{\rho_l}Re$, is the particle Reynolds number times a constant (approximately 0.7) since the density ratio of the sphere and the liquid is a constant.

A listing of the experimental cases and associated parameters are given in Table (2.2). In all the cases, the particle bounced at least twice. The impact Stokes number for each first collision was larger than 10. The maximum height achieved in the rebound motion is lower than the initial height, which is the result of viscous losses and inelasticity.

Case	$h(t=0)$	$h(t=0)/D$	Re_I	St_I	Re_{II}	St_{II}	Re_{III}	St_{III}	Re_{IV}	St_{IV}
1	5.5mm	0.58	53	38	26	19	9	7	-	-
2	10.5mm	1.10	75	54	39	28	20	15	-	-
3	15.2mm	1.60	90	65	50	36	25	18	-	-
4	19.6mm	2.06	104	75	58	42	35	25	12	8
5	25.3mm	2.66	113	81	65	46	37	26	12	9
6	28.4mm	2.98	123	88	69	50	42	30	13	9
7	35.7mm	3.75	127	92	70	51	43	31	15	10

Table 2.2: Experiments with particle Reynolds numbers and Stokes numbers at the first impact (I), the second impact (II), the third impact (III) and the forth impact (IV).

2.3.1 Trajectories for the sphere

The trajectories for a sphere dropped from different distances are compared in figure (2.8). Ideally, the initial falling process from the release surface for each case should coincide. The deviation results from the uncertainty of the experiments; the maximum error is less than 3%. In examing the rebound, the maximum height achieved in the first rebound increases as the initial drop height increases; the time duration from the first collision to the second collision also increases with drop height.

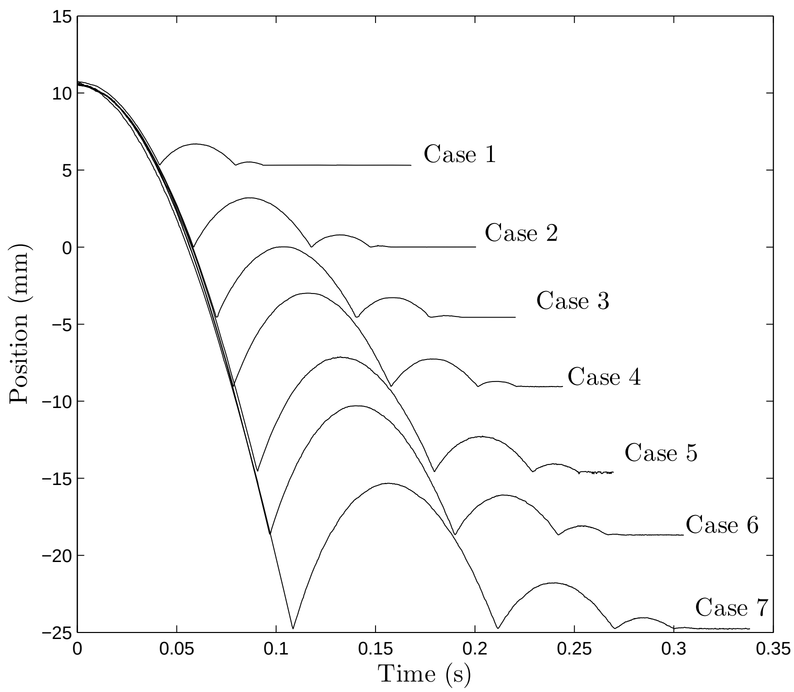

Figure 2.8: Particle trajectories for the given different cases described in Table (2.2).

The measured trajectories are used to calibrate and validate a contact model proposed in the Chapter 4.

2.3.2 Velocity decrease prior to the collision

A velocity decrease is observed when the velocity of the particle is plotted as a function of the gap between the particle and the wall as shown in figure (2.9). The velocity is calculated as the time derivative of the fitting curve. In figure 2.9(a), the sphere starts from zero velocity at a certain distance away from the wall. It accelerates under gravity and approaches the wall. When it is about to collide with the wall, the velocity decreases. Figure 2.9(b) shows the enlarged detail part: the velocity starts to decrease when the gap decreases below 0.12D. This unique behavior of the impacting sphere does not occur in a dry collision process when the surrounding medium effect is negligible. Joseph *et al.* (2001) observed this velocity decrease prior to the collision in their pendulum-wall collision experiments since there was negligible gravitational acceleration in the horizontal collision between a pendulum and a vertical wall. Gondret *et al.* (2002) who performed the similar experiments of a settling sphere did not obtain the velocity decrease because they used a lower frame rate for the recording camera, 500 fps. When picking data with 500 fps (2 ms interval between two successive points), the detailed behavior of the impacting sphere is missed, especially when it is close to the wall. The velocity decrease cannot be observed, as shown in figure (2.10). Thus a higher frame rate is required to capture this unique behavior of the impacting sphere in a liquid environment.

This velocity decrease is more obvious for a settling process with a smaller Reynolds number. Using the current experiment setup and changing the liquid to pure glycerol, for which the viscosity of the liquid increases to 1.15 Pa·s^{-1} (more than 20 times higher), the same sphere released from zero velocity settles toward the Zerodur wall and rests there without rebound. The Reynolds number of the sphere based on the terminal velocity is $Re = \frac{D\tilde{V}_{\infty}}{\nu} = 0.67$. The corresponding trajectory is plotted in figure (2.11). The existence of the solid wall interrupts the falling of the sphere, and the effect of the surrounding liquid with this additional solid boundary makes the sphere come to rest in front of the wall.

When plotting the velocity as a function of the gap between the sphere and the wall, the critical distance when the velocity starts to decrease is about one diameter, as shown in figure (2.12). The solid line shown in the figure (2.12) is a calculation of the velocity of a sphere falling in the same surrounding liquid environment without the existence of the solid wall. The falling velocity is

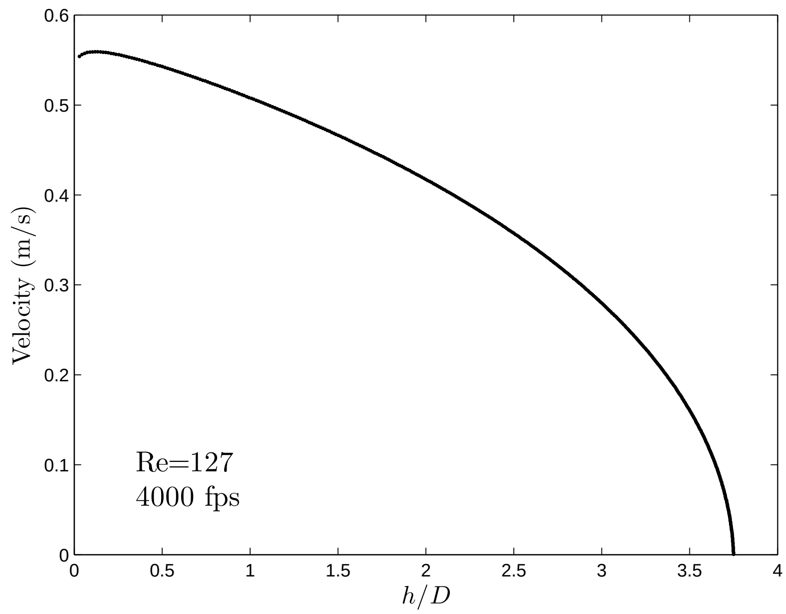

(a)

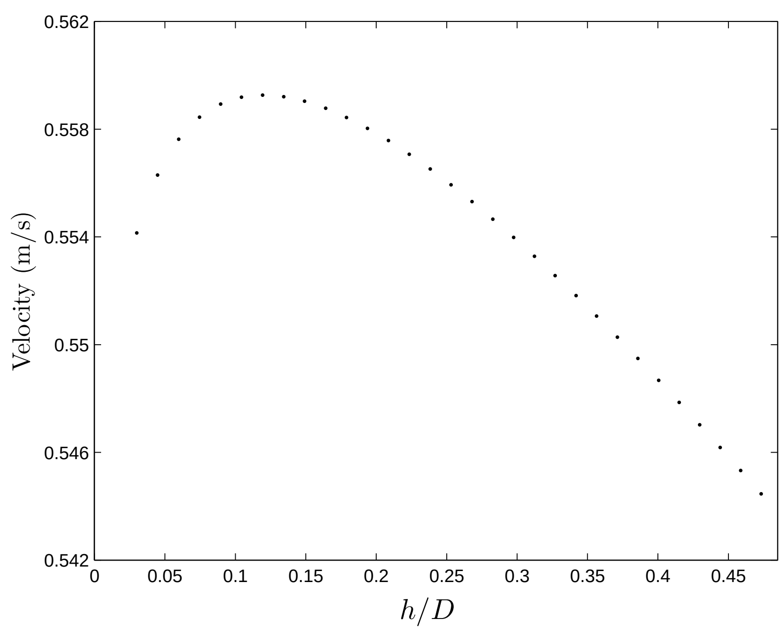

(b)

Figure 2.9: Velocity of the impacting sphere in case 7 with the frame rate 4000 fps. (b) shows the enlarged detail part of (a) when the sphere is about to collide with the wall.

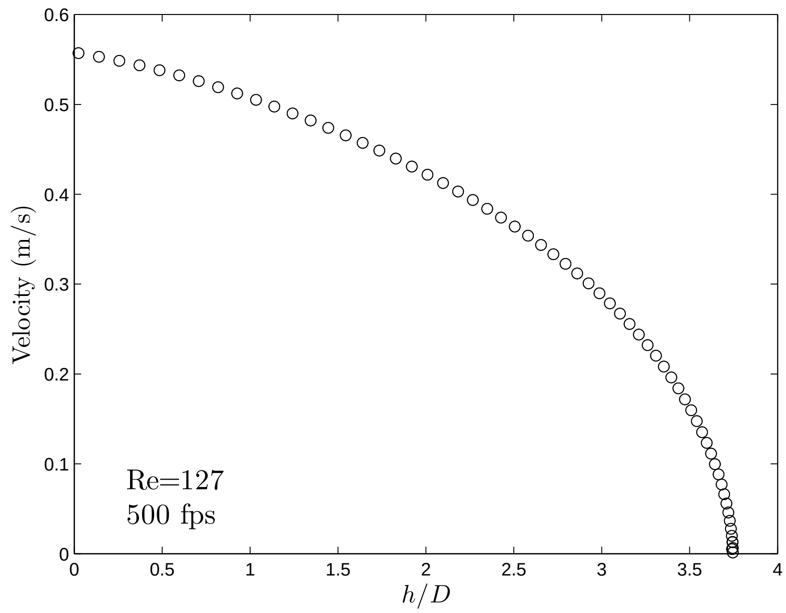

Figure 2.10: Velocity of the impacting sphere in case 7 with the frame rate 500 fps.

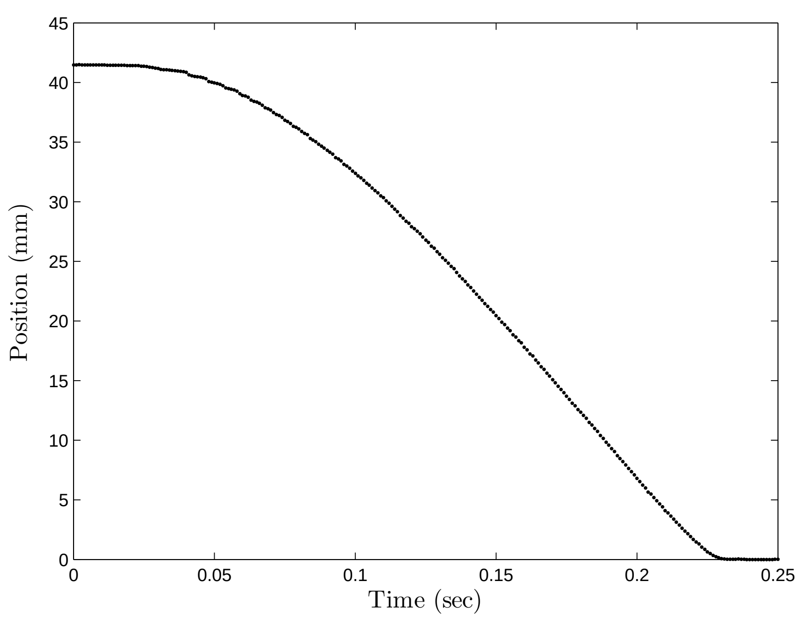

Figure 2.11: Trajectory of a sphere settling on the wall.

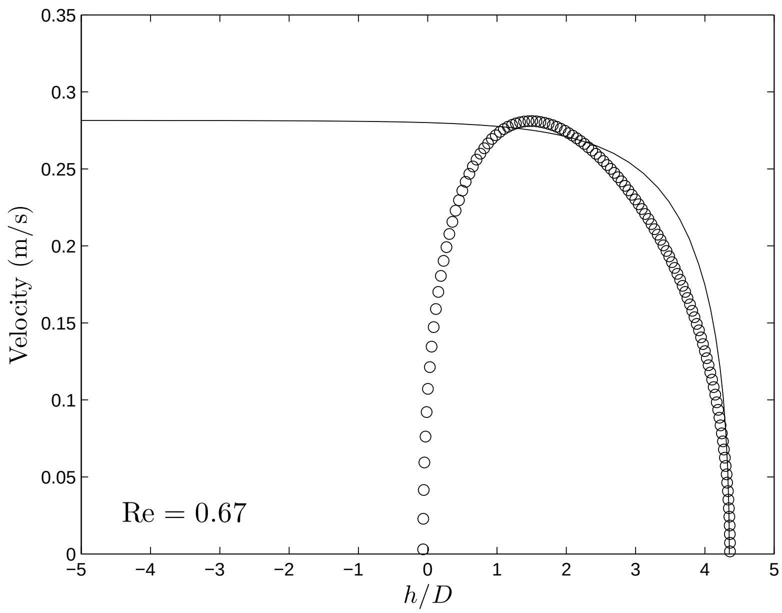

Figure 2.12: Velocity of a sphere settling on the wall with $Re = 0.67$ as a function of the gap between the sphere and the wall.

calculated analytically by solving the equation of motion for a sphere with a low Reynolds number:

$$m_p \frac{d\tilde{V}}{d\tilde{t}} = m_p g - m_l g - F_D$$

where $F_D = 6\pi\mu a V$ is the Stokes drag for the sphere and a is the radius of the sphere. The motion equation can be simplified as an ordinary differential equation for the velocity $\tilde{V}$:

$$\frac{d\tilde{V}}{d\tilde{t}} = g(1 - \frac{\rho_l}{\rho_p}) - \frac{6\pi\mu a}{\frac{4}{3}\pi a^3 \rho_p}\tilde{V}.$$

The velocity of the particle measured from the experiment follows the analytical trend when the gap is large ($h/D > 1$). The deviation is resulted from the omission of the added mass and history force in the equation of the particle motion. When the velocity is increasing, the added mass and history force have noticeable influence on the motion of the particle. These two forces disappear after the terminal velocity is achieved. It is obvious in the figure (2.12) that the velocity decreases after the distance between the sphere and the wall is less than one diameter.

2.3.3 Coefficient of restitution

The coefficient of restitution of each collision, e, is calculated as the ratio of the averaged rebound velocity to the averaged impact velocity over 2 ms time interval. Figure (2.13) shows the semi-log relation between e and the particle impact Stokes number, St, and the result is compared with the observations for steel sphere and Zerodur wall reported by Joseph *et al.* (2001) and Gondret *et al.* (2002). The results from the current experiments present more data for Stokes number ranging from 1 to 100 which is deficient in the previous literature.

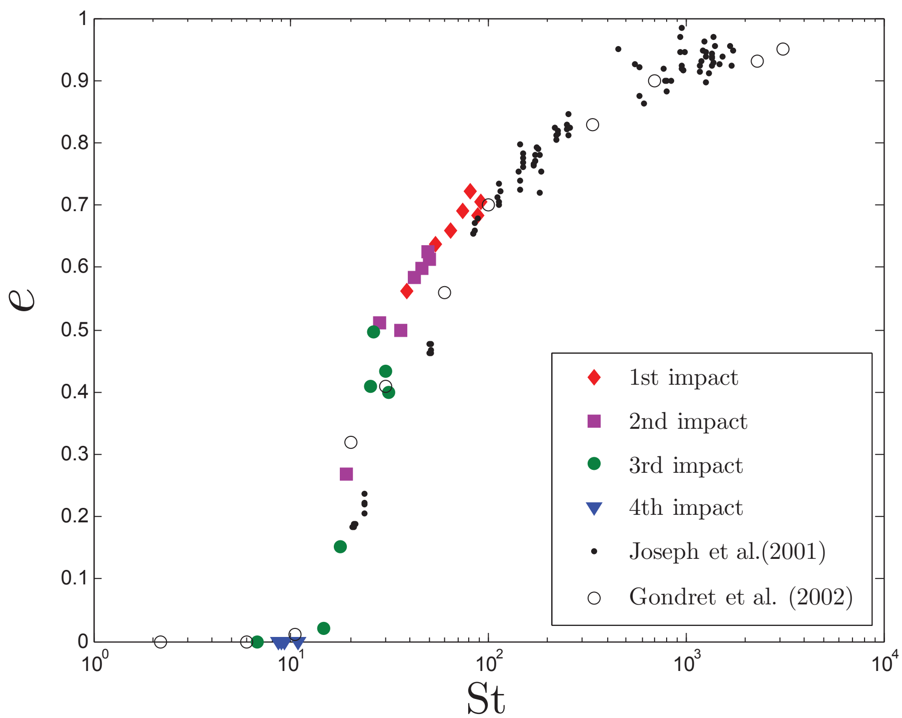

Figure 2.13: Coefficient of restitution for the first and second collisions.

As shown in figure (2.13), the coefficient of restitution is a function of the particle impact Stokes number and agrees with the previous conclusion found by other researchers. For Stokes number less than 10 (all the 4th impacts and one third impact), the coefficient of restitution is zero and there is no visible rebound. As Stokes number increases, the value of e increases with large slope for Stokes number ranging from 10 to 100.

For the Stokes numbers ranging from 20 to 50, the results reported by Joseph *et al.* (2001)

are lower than the current experimental results and the results in Gondret *et al.* (2002). This can be explained by the technique used to evaluate the coefficient of restitution. The coefficient of restitution is calculated as a ratio of the rebound velocity to the impact velocity. The rebound and impact velocities in the current experiments and in Gondret *et al.* (2002) are calculated as the time derivative of the measured trajectory $\triangle h/\triangle t$ with time interval $\triangle t = 2$ ms. The rebound and impact velocities in Joseph *et al.* (2001) were taken as the slopes of the fitted lines over 5 to 10 points (depending on the framing rate that varies from 500 fps to 2000 fps) on the position-time diagram as shown in figure (3.3) so that the obtained velocities are averaged values over 5$\sim$10 ms time interval. The actual collision duration is typically 0.01 ms (measured by Gondret *et al.* (2002) with a piezoelectric sensor). Thus, the coefficient of restitution obtained from all of the experiments is an effective macroscopic value. An average over a longer time interval attenuates the fact that the velocity decreases under the effect of the interstitial liquid so that it produces a larger impact velocity and a lower coefficient of restitution. The difference is more obvious when the liquid is more viscous with Stokes numbers lower than 50. Thus, to capture the actual slowdown for a rapid collision, the time interval cannot be too long. However, the time interval cannot be too short either. The experimental technique, such as the recording rate, limits the minimum time interval. A more important reason is a time interval shorter than 2 ms does not reflect the real approaching velocity but pronounces only the decelerating particle motion.